Study on spontaneous emission in complex multilayered plasmonic system via surface integral equation approach with layered medium Green's function

Yongpin P. Chen,[1] Wei E. I. Sha,[2] Wallace C. H. Choy,[2] Lijun Jiang,[2] and Weng Cho Chew[3,*]

[1]*School of Electronic Engineering, University of Electronic Science and Technology of China, Chengdu, China*
[2]*Department of Electrical and Electronic Engineering, University of Hong Kong, Hong Kong, China*
[3]*Department of Electrical and Computer Engineering University of Illinois, Urbana-Champaign, Illinois, USA*

[*]*w-chew@uiuc.edu*

Abstract: A rigorous surface integral equation approach is proposed to study the spontaneous emission of a quantum emitter embedded in a multi-layered plasmonic structure with the presence of arbitrarily shaped metallic nanoscatterers. With the aid of the Fermi's golden rule, the spontaneous emission of the emitter can be calculated from the local density of states, which can be further expressed by the imaginary part of the dyadic Green's function of the whole electromagnetic system. To obtain this Green's function numerically, a surface integral equation is established taking into account the scattering from the metallic nanoscatterers. Particularly, the modeling of the planar multilayered structure is simplified by applying the layered medium Green's function to reduce the computational domain and hence the memory requirement. Regarding the evaluation of Sommerfeld integrals in the layered medium Green's function, the discrete complex image method is adopted to accelerate the evaluation process. This work offers an accurate and efficient simulation tool for analyzing complex multilayered plasmonic system, which is commonly encountered in the design of optical elements and devices.

© 2012 Optical Society of America

OCIS codes: (050.1755) Computational electromagnetic methods; (260.2110) Electromagnetic optics; (350.4238) Nanophotonics and photonic crystals; (240.6680) Surface plasmons.

References and links

1. L. Rogobete, F. Kaminski, M. Agio, and V. Sandoghdar, "Design of plasmonic nanoantennae for enhancing spontaneous emission," Opt. Lett. **32**, 1623–1625 (2007).
2. M. A. Noginov, H. Li, Yu. A. Barnakov, D. Dryden, G. Nataraj, G. Zhu, C. E. Bonner, M. Mayy, Z. Jacob, and E. E. Narimanov, "Controlling spontaneous emission with metamaterials," Opt. Lett. **35**, 1863–1865 (2010).
3. P. Lodahl, A. F. van Driel, I. S. Nikolaev, A. Irman1, K. Overgaag, D. Vanmaekelbergh, and W. L. Vos, "Controlling the dynamics of spontaneous emission from quantum dots by photonic crystals," Nature **430**, 654–657 (2004).
4. E. M. Purcell, "Spontaneous emission probabilities at radio frequencies," Phys. Rev. **69**, 681 (1946).
5. C. Gerry and P. Knight, *Introductory Quantum Optics* (Cambridge University Press, 2005).

#172033 - $15.00 USD Received 5 Jul 2012; revised 10 Aug 2012; accepted 11 Aug 2012; published 20 Aug 2012

6. L. Novotny and B. Hecht, *Principles of Nano-optics* (Cambridge University Press, 2006).
7. K. Okamoto, I. Niki, A. Shvartser, Y. Narukawa, T. Mukai, and A. Scherer, "Surface-plasmon-enhanced light emitters based on InGaN quantum wells," Nat. Mater. **3**, 601–605 (2004).
8. J.-J. Greffet, "Nanoantennas for light emission," Science **308**, 1561–1563 (2005).
9. A. G. Curto, G. Volpe, T. H. Taminiau, M. P. Kreuzer, R. Quidant, and N. F. van Hulst, "Unidirectional emission of a quantum dot coupled to a nanoantenna," Science **329**, 930–933 (2010).
10. K. G. Lee, X. W. Chen, H. Eghlidi, P. Kukura, R. Lettow, A. Renn, V. Sandoghdar, and S. Götzinger, "A planar dielectric antenna for directional single-photon emission and near-unity collection efficiency," Nat. Photo. **5**, 166–169 (2011).
11. J. Li, A. Salandrino, and N. Engheta, "Shaping light beams in the nanometer scale: A Yagi-Uda nanoantenna in the optical domain," Phys. Rev. B **76**, 245403 (2007).
12. X. W. Chen, W. C. H. Choy, S. He, and P.C. Chui, "Comprehensive analysis and optimal design of top-emitting organic light emitting devices," J. Appl. Phys. **101**, 113107 (2007).
13. X. W. Chen, W. C. H. Choy, and S. He, "Efficient and rigorous modeling of light emission in planar multilayer organic light-emitting diodes," IEEE/OSA J. Display Technol. **3**, 110–117 (2007).
14. W. C. Chew, J. M. Jin, E. Michielssen, and J. M. Song, *Fast and Efficient Algorithms in Computational Electromagnetics* (Artech House, Norwood, 2001).
15. K. Yee, "Numerical solution of initial boundary value problems involving Maxwell's equations in isotropic media," IEEE Trans. Antennas Propag. **14**, 302–307 (1966).
16. P. Monk, *Finite Element Methods for Maxwell's Equations* (Oxford University Press, 2003).
17. W. C. Chew, M. S. Tong, and B. Hu, *Integral Equations for Electromagnetic and Elastic Waves* (Morgan & Claypool Publishers, 2009).
18. A. M. Kern and O. J. F. Martin, "Surface integral formulation for 3D simulations of plasmonic and high permittivity nanostructures," J. Opt. Soc. Am. A **26**, 732–740 (2009).
19. B. Gallinet, A. M. Kern, and O. J. F. Martin, "Accurate and versatile modeling of electromagnetic scattering on periodic nanostructures with a surface integral approach," J. Opt. Soc. Am. A **27**, 2261–2271 (2010).
20. J. M. Taboada, J. Rivero, F. Obelleiro, M. G. Araújo, and L. Landesa, "Method-of-moments formulation for the analysis of plasmonic nano-optical antennas," J. Opt. Soc. Am. A **28**, 1341–1348 (2011).
21. M. G. Araújo, J. M. Taboada, D. M. Solís, J. Rivero, L. Landesa, and F. Obelleiro, "Comparison of surface integral equation formulations for electromagnetic analysis of plasmonic nanoscatterers," Opt. Express **20**, 9161–9171 (2012).
22. K. A. Michalski and J. R. Mosig, "Multilayered media Green's functions in integral equation formulations," IEEE Trans. Antennas Propagat. **45**, 508–519 (1997).
23. Y. P. Chen, W. C. Chew, and L. Jiang, "A new Green's function formulation for modeling homogeneous objects in layered medium," IEEE Trans. Antennas Propagat. accepted for publication.
24. D. G. Fang, J. J. Yang, and G. Y. Delisle, "Discrete image theory for horizontal electric dipoles in a multilayered medium," Proc. Inst. Elect. Eng. **135**, 297–303 (1988).
25. E. N. Economou, *Green's Functions in Quantum Physics* (Springer, Berlin, 2006).
26. R. Carminati, J.-J. Greffet, C. Henkel, and J.M. Vigoureux, "Radiative and non-radiative decay of a single molecule close to a metallic nanoparticle," Opt. Comm. **261**, 368–375, 2006.
27. W. C. Chew, *Waves and Fields in Inhomogeneous Media* (Van Nostrand Reinhold, 1990; IEEE Press, 1995).
28. X. W. Chen, M. Agio, and V. Sandoghdar, "Metallodielectric hybrid antennas for ultrastrong enhancement of spontaneous emission," Phys. Rev. Lett. **108**, 233001 (2012).
29. A. J. Poggio and E. K. Miller, "Integral equation solutions of three dimensional scattering problems," in *Computer Techniques for Electromagnetics* (Permagon, 1973).
30. Y. Chang and R. Harrington, "A surface formulation for characteristic modes of material bodies," IEEE Trans. Antennas Propag. **25**, 789–795 (1977).
31. T.-K. Wu and L. L. Tsai, "Scattering from arbitrarilyshaped lossy dielectric bodies of revolution," Radio Sci. **12**, 709–718 (1977).
32. S. M. Rao, D. R. Wilton, and A. W. Glisson, "Electromagnetic scattering by surface of arbitrary shape," IEEE Trans. Antennas Propagat. **30**, 409–418 (1982).
33. W. C. Chew, J. L. Xiong, and M. A. Saville, "A matrix-friendly formulation of layered medium Green's function," IEEE Antennas Wireless Propagat. Lett. **5**, 490–494 (2006).
34. T. K. Sarkar and O. Pereira, "Using the matrix pencil method to estimate the parameters of a sum of complex exponentials," lEEE Antennas Propagat. Magazine **37**, 48–55 (1995).
35. A. Alparslan, M. I. Aksun, and K. A. Michalski, "Closed-form Green's functions in planar layered media for all ranges and materials," IEEE Trans. Microw. Theory Tech. **58**, 602–613 (2010).
36. Y. P. Chen, W. C. Chew, and L. Jiang, "A novel implementation of discrete complex image method for layered medium Green's function," IEEE Antennas Wireless Propagat. Lett. **10**, 419–422 (2011).
37. A. D. Rakic, A. B. Djurisic, J. M. Elazar, and M. L. Majewski, "Optical properties of metallic films for vertical-cavity optoelectronic devices," Appl. Opt. **37**, 5271–5283 (1998).
38. G. Mie, "Beiträge zur optik trüber medien, speziell kolloidaler metallösungen," Ann. Phys. **25**, 377–445 (1908).

#172033 - $15.00 USD Received 5 Jul 2012; revised 10 Aug 2012; accepted 11 Aug 2012; published 20 Aug 2012
(C) 2012 OSA

39. A. Kinkhabwala, Z. Yu, S. Fan, Y. Avlasevich, K. Müllen, and W. E. Moerner, "Large single-molecule fluorescence enhancements produced by a bowtie nanoantenna," Nat. Photo. **3**, 654–657 (2009).

1. Introduction

The control of spontaneous light emission plays an important role in designing various optical elements and devices, such as nanoantenna, hyperbolic metamaterial, light-emitting diode (LED), laser, solar cell, etc [1–3]. Inhibiting unwanted spontaneous emission (SE) and boosting desired ones will promote emerging optical designs with new functionalities. It is well known that atoms at the excited states can spontaneously emit light even in the vacuum. Purcell in 1946 first demonstrated that the SE of a quantum emitter is not an intrinsic property of the emitter but can be modified when it is coupled to a cavity resonator, now known as the Purcell effect [4]. SE can be explained by the atom-field interaction in the weak-coupling regime through the quantization of the electromagnetic (EM) field. The vacuum fluctuation of the EM field perturbs the atom system and induces the "spontaneous" emission of photons. If the local EM environment is properly modified, which leads to the change of local density of states (LDOS), SE can be manipulated. The spontaneous emission rate (SER) expressed by the Fermi's golden rule [5] can be related to the LDOS in the local EM environment. The LDOS can further be expressed in terms of the imaginary part of the dyadic Green's function [6]. Finding the SER is equivalent to calculating the Green's tensor in inhomogeneous EM environment. Therefore, this quantum electrodynamic problem can finally be cast into a classical EM scattering problem.

As one of the methods to control SE, plasmonic effects are successfully explored to design various optical elements and devices for enhancing and redirecting the emission [7–10]. Regarding laser and light emitting diode applications, enhancing SE enables the improved photoluminescence, low threshold current and fast turn-on time due to the strong optical confinement by plasmon resonances. Meanwhile, SE can be redirected with strong directionality in Yagi-Uda nanoantenna system, which is quite useful in molecular detection and sensing [11]. On one hand, the multilayered structure is commonly encountered in the above designs which strongly affect their optical response. The multilayer substrate will significantly modify the radiation pattern and directionality of the optical antenna. In multilayer devices, the thickness of each layer will determine the spectral and spatial locations of waveguide modes, which can be coupled to plasmonic resonances [12, 13]. On the other hand, modeling SE of multilayer structure gives rise to computational challenges in finding the dyadic Green's function. From computational electromagnetics [14] point of view, there are a wide variety of numerical methods available for achieving this purpose. The differential-equation-based methods [15, 16] are straightforward in implementation, but require one to discretize the scatterers as well as the background, leading to a large computational domain. The integral-equation-based methods [17] only discretize the scatterers and thus does not require any domain truncation or absorbing boundary condition with more accurate results compared to differential-equation-based methods. Also, if the surface equivalence principle is applied, the surface integral equation (SIE), also known as boundary element method (BEM), can be obtained, where the unknowns are only defined on the boundary of the scatterers. Due to these unique features, SIE receives intensive research in plasmonic nanostructures [18–21].

In this paper, the SIE is adopted to calculate the SER of a complex multilayered plasmonic system, where the quantum emitter can be embedded in an selected layer with the presence of arbitrarily shaped metallic nanoparticles. Surface discretization is implemented only at the boundary of the nanoparticles and the effects from multilayer structure is accounted for by utilizing the layered medium Green's function (LMGF) [22, 23]. Compared to the SIE based on free-space Green's function (FSGF) and other differential equation based approaches, the modeling complexity in dealing with such a complex multilayered plasmonic structure can be

#172033 - $15.00 USD Received 5 Jul 2012; revised 10 Aug 2012; accepted 11 Aug 2012; published 20 Aug 2012
(C) 2012 OSA

greatly reduced. Because the multilayered structure can be viewed as the background and corresponding scattering effects are included in the LMGF itself, without the necessity of discretization. For the evaluation of Sommerfeld integrals in the LMGF, which are infinite, oscillatory and slowly convergent integrals, the discrete complex image method (DCIM) [24] is further applied to reduce the computational cost. The work develops an accurate and efficient simulation tool for predicting SE of a quantum emitter in the complex multilayered plasmonic system.

2. Theoretical principles

2.1. Green's function approach in spontaneous emission

According to quantum electrodynamics, a quantum emitter (atom, molecule or quantum dot, etc) at excited states spontaneously emits photons in inhomogeneous environment due to the ground-state (vacuum) fluctuations of the EM field. If we consider the emitter to be a two-level system located at $\mathbf{r} = \mathbf{r}_0$ and with the transition dipole moment operator $\hat{\mathbf{p}} = -e\hat{\mathbf{r}} = \mathbf{p}\left(|g\rangle\langle e| + |e\rangle\langle g|\right)$, the SER of this system can be determined by the Fermi's golden rule [6],

$$\gamma = \frac{\pi\omega_0}{\hbar\varepsilon_0}|\mathbf{p}|^2 \sum_k \left[\mathbf{n}_p \cdot (\mathbf{u}_\mathbf{k}\mathbf{u}_\mathbf{k}^*) \cdot \mathbf{n}_p\right] \delta(\omega_\mathbf{k} - \omega_0) \tag{1}$$

where $\mathbf{p} = \langle g|\hat{\mathbf{p}}|e\rangle = \langle e|\hat{\mathbf{p}}|g\rangle$ and $\mathbf{u}_\mathbf{k}$ are the normalized eigenmodes of photons satisfying the following Helmholtz equations

$$\nabla \times \nabla \times \mathbf{u}_\mathbf{k}(\mathbf{r}, \omega_\mathbf{k}) - \frac{\omega_\mathbf{k}^2}{c^2}\mathbf{u}_\mathbf{k}(\mathbf{r}, \omega_\mathbf{k}) = 0 \tag{2}$$

We can then define the electric-type Green's function that satisfies the same equation with the excitation of delta function

$$\nabla \times \nabla \times \bar{\mathbf{G}}(\mathbf{r}, \mathbf{r}', \omega) - \frac{\omega^2}{c^2}\bar{\mathbf{G}}(\mathbf{r}, \mathbf{r}', \omega) = \bar{\mathbf{I}}\delta(\mathbf{r} - \mathbf{r}') \tag{3}$$

According to the eigenmode expansion approach, the Green's function can be expressed as the summation of the eigenmodes [25]

$$\mathrm{Im}\left[\bar{\mathbf{G}}(\mathbf{r}, \mathbf{r}', \omega)\right] = \frac{\pi c^2}{2\omega}\sum_k \mathbf{u}_\mathbf{k}(\mathbf{r}, \omega_\mathbf{k})\mathbf{u}_\mathbf{k}^*(\mathbf{r}', \omega_\mathbf{k})\delta(\omega - \omega_\mathbf{k}) \tag{4}$$

Hence, the SER can be determined by the Green's function

$$\gamma(\mathbf{r}_0, \omega_0) = \frac{2\omega_0^2}{\hbar\varepsilon_0 c^2}|\mathbf{p}|^2\{\mathbf{n}_p \cdot \mathrm{Im}\left[\bar{\mathbf{G}}(\mathbf{r}_0, \mathbf{r}_0, \omega_0)\right] \cdot \mathbf{n}_p\} \tag{5}$$

If the emitter has no fixed dipole axis and the EM environment is isotropic, the emission rate is obtained by averaging over all possible orientations.

$$\gamma(\mathbf{r}_0, \omega_0) = \frac{2\omega_0^2}{3\hbar\varepsilon_0 c^2}\mathrm{Im}\{\mathrm{Tr}\left[\bar{\mathbf{G}}(\mathbf{r}_0, \mathbf{r}_0, \omega_0)\right]\} \tag{6}$$

In this case, the averaged SER is related to the LDOS [6] defined by

$$\rho(\mathbf{r}_0, \omega_0) = \sum_\mathbf{k}|\mathbf{u}_\mathbf{k}|^2\delta(\omega_\mathbf{k} - \omega_0) = \frac{2\omega_0}{\pi c^2}\mathrm{Im}\{\mathrm{Tr}\left[\bar{\mathbf{G}}(\mathbf{r}_0, \mathbf{r}_0, \omega_0)\right]\} \tag{7}$$

#172033 - $15.00 USD Received 5 Jul 2012; revised 10 Aug 2012; accepted 11 Aug 2012; published 20 Aug 2012
(C) 2012 OSA

To quantify the SE enhancement in the inhomogeneous environment, it is convenient to define the normalized SER or Purcell factor as

$$\frac{\gamma}{\gamma_0} = \frac{\rho(\mathbf{r}_0,\omega_0)}{\rho_0(\mathbf{r}_0,\omega_0)} = \frac{\mathrm{Im}\{\mathrm{Tr}\left[\bar{\mathbf{G}}(\mathbf{r}_0,\mathbf{r}_0,\omega_0)\right]\}}{\mathrm{Im}\{\mathrm{Tr}\left[\mathbf{G}_0(\mathbf{r}_0,\mathbf{r}_0,\omega_0)\right]\}} \tag{8}$$

Here $\bar{\mathbf{G}}_0$ is the FSGF, where the surrounding medium is homogeneous and unbounded. In summary, the local environment changes the eigenmodes of the EM field, and thus modifies the LDOS. By calculating the Green's function, and making the source point and the observation point identical ($\mathbf{r} = \mathbf{r}' = \mathbf{r}_0$), one can obtain the LDOS and SER.

The SER here contains both radiative and nonradiative parts. Since the normalized SER is equivalent to the normalized power emitted by a classical dipole, one can first obtain the nonradiative SER, which is proportional to the power absorbed by the environment, through near field calculation. After that, the radiative one can be easily obtained by subtraction according to energy conservation [26].

2.2. Surface integral equation with layered medium Green's function

As has been discussed, the computation of SER is equivalent to the calculation of Green's function . However, for arbitrary inhomogeneous environment, finding the Green's function is nontrivial and can only be realized via a rigorous full-wave EM solver. In the following, we will apply the SIE with LMGF to obtain the SER of the hybrid plasmonic system.

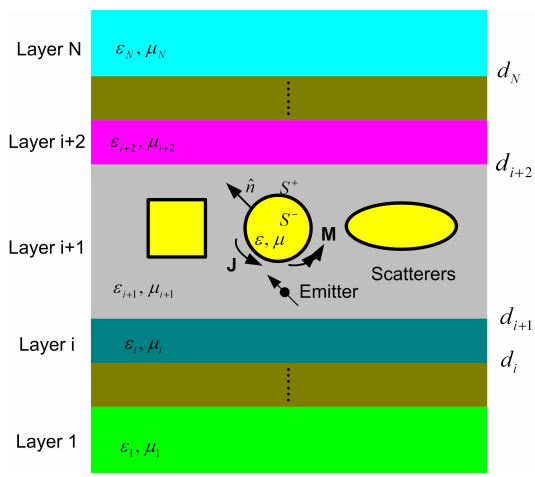

Fig. 1. Configuration profile: arbitrarily shaped nano particles embedded in a multilayered structure. Surface integral equation can be set up by invoking the surface equivalence principle. With the help of LMGF, only the surfaces of the scatterers excluding the substrate need discretization.

The schematic configuration is shown in Fig. 1, where the nanoscatterers with arbitrary shapes are embedded in a multilayered structure. To setup the SIE, the integral operator is first introduced to describe the electric/magnetic field (**E**/**H**) generated by equivalent electric/magnetic currents (**J**/**M**) [17]

$$\mathbf{E}(\mathbf{r}) = \mathscr{L}_{\mathrm{E}}(\mathbf{r},\mathbf{r}')\cdot\mathbf{J}(\mathbf{r}') + \mathscr{K}_{\mathrm{E}}(\mathbf{r},\mathbf{r}')\cdot\mathbf{M}(\mathbf{r}') \tag{9}$$

$$\mathbf{H}(\mathbf{r}) = \mathscr{L}_{\mathrm{H}}(\mathbf{r},\mathbf{r}')\cdot\mathbf{M}(\mathbf{r}') + \mathscr{K}_{\mathrm{H}}(\mathbf{r},\mathbf{r}')\cdot\mathbf{J}(\mathbf{r}') \tag{10}$$

#172033 - $15.00 USD Received 5 Jul 2012; revised 10 Aug 2012; accepted 11 Aug 2012; published 20 Aug 2012
(C) 2012 OSA

where

$$\mathscr{L}_{\mathrm{E}}(\mathbf{r},\mathbf{r}')\cdot = i\omega \int d\mathbf{r}'\bar{\mathbf{G}}_e(\mathbf{r},\mathbf{r}')\mu(\mathbf{r}')\cdot \tag{11}$$

$$\mathscr{K}_{\mathrm{H}}(\mathbf{r},\mathbf{r}')\cdot = \mu^{-1}(\mathbf{r}) \int d\mathbf{r}'\nabla\times\bar{\mathbf{G}}_e(\mathbf{r},\mathbf{r}')\mu(\mathbf{r}')\cdot \tag{12}$$

$$\mathscr{L}_{\mathrm{H}}(\mathbf{r},\mathbf{r}')\cdot = i\omega \int d\mathbf{r}'\bar{\mathbf{G}}_m(\mathbf{r},\mathbf{r}')\varepsilon(\mathbf{r}')\cdot \tag{13}$$

$$\mathscr{K}_{\mathrm{E}}(\mathbf{r},\mathbf{r}')\cdot = -\varepsilon^{-1}(\mathbf{r}) \int d\mathbf{r}'\nabla\times\bar{\mathbf{G}}_m(\mathbf{r},\mathbf{r}')\varepsilon(\mathbf{r}')\cdot \tag{14}$$

We only discuss the electric-type LMGF $\bar{\mathbf{G}}_e$ in Eq. (11) and Eq. (12) here since the magnetic-type LMGF $\bar{\mathbf{G}}_m$ in Eq. (13) and Eq. (14) can be easily obtained via the duality principle [27]. The $\bar{\mathbf{G}}_e$ is defined as

$$\bar{\mathbf{G}}_e(\mathbf{r},\mathbf{r}') = \bar{\mathbf{G}}_e^{\mathrm{TE}}(\mathbf{r},\mathbf{r}') + \frac{1}{k_{nm}^2}\bar{\mathbf{G}}_e^{\mathrm{TM}}(\mathbf{r},\mathbf{r}') \tag{15}$$

where $k_{nm}^2 = \omega^2\varepsilon_n\mu_m$, m and n are the layer indices of the source and observation points, and

$$\bar{\mathbf{G}}_e^{\mathrm{TE}}(\mathbf{r},\mathbf{r}') = (\nabla\times\hat{z})(\nabla'\times\hat{z})\frac{i}{4\pi}\int_0^\infty dk_\rho J_0(k_\rho\rho)\frac{F^{\mathrm{TE}}(k_\rho,z,z')}{k_{mz}k_\rho} \tag{16}$$

$$\bar{\mathbf{G}}_e^{\mathrm{TM}}(\mathbf{r},\mathbf{r}') = (\nabla\times\nabla\times\hat{z})\left(\nabla'\times\nabla'\times\hat{z}\right)\frac{i}{4\pi}\int_0^\infty dk_\rho J_0(k_\rho\rho)\frac{F^{\mathrm{TM}}(k_\rho,z,z')}{k_{mz}k_\rho} \tag{17}$$

Here $F^{\mathrm{TE/TM}}(k_\rho,z,z')$ is the propagation factor in the layered medium [27], $k_{mz} = \sqrt{k_m^2 - k_\rho^2}$, and $J_0(k_\rho\rho)$ is the zeroth order Bessel function.

We will focus our attention on the situation where the emitter and the nanoscatterers are put in the same layer. However, it can be easily extended to the cases where they are in different layers by properly adjusting the propagation factor. Such device in enhancing SE is recently reported in [28].

Since metallic nanoparticles are penetrable at the optical frequency band, the assumption of perfectly electric conductor (PEC) in microwave spectrums is no longer valid; and the PMCHWT (Poggio, Miller, Chang, Harrington, Wu, Tsai) formulation [29–31] should be applied to account for the conductive (ohmic) loss of metal

$$\left.\begin{bmatrix} -\mathbf{E}_{\mathrm{inc}}^o \\ -\mathbf{H}_{\mathrm{inc}}^o \end{bmatrix}\right|_{\tan} = \begin{bmatrix} \left(\mathscr{L}_E^o + \mathscr{L}_E^i\right) & \left(\mathscr{K}_E^o + \mathscr{K}_E^i\right) \\ \left(\mathscr{K}_H^o + \mathscr{K}_H^i\right) & \left(\mathscr{L}_H^o + \mathscr{L}_H^i\right) \end{bmatrix} \cdot \left.\begin{bmatrix} \mathbf{J} \\ \mathbf{M} \end{bmatrix}\right|_{\tan} \tag{18}$$

where the superscript "o" means outside the boundary of the scatterer and "i" means inside the boundary. The subscript "tan" means tangential component. The incident field is evaluated in the presence of the layered medium and in the absence of the metallic scatterer. Once the equivalent electric/magnetic currents are solved, the scattered field can be easily obtained via Eq. (9) and Eq. (10).

To model arbitrarily shaped nanoscatterers, the triangular surface mesh and the RWG (Rao-Wilton-Glisson) basis functions [32] defined on it are utilized. By applying the RWG bases as the expansion and testing functions, the LMGF can be cast into a matrix-friendly form, where the singularity of the dyadic Green's function becomes much weaker through transferring the partial derivatives from the Green's function to the basis functions [23, 33]. The matrix

#172033 - $15.00 USD Received 5 Jul 2012; revised 10 Aug 2012; accepted 11 Aug 2012; published 20 Aug 2012
(C) 2012 OSA

representation of $\mathscr{L}_{\mathrm{E}}$ is

$$\begin{aligned}
& \langle \mathbf{f}_j(\mathbf{r}), \mathscr{L}_E(\mathbf{r},\mathbf{r}'), \mathbf{f}_i(\mathbf{r}')\rangle \\
= \; & i\omega\mu_m \langle \mathbf{f}_{js}(\mathbf{r}), g_{e,ss}(\mathbf{r},\mathbf{r}'), \mathbf{f}_{is}(\mathbf{r}')\rangle \\
+ \; & i\omega\mu_m \langle \hat{z}\cdot\mathbf{f}_j(\mathbf{r}), g_{e,zz}(\mathbf{r},\mathbf{r}'), \hat{z}\cdot\mathbf{f}_i(\mathbf{r}')\rangle \\
+ \; & i\omega\mu_m \langle \hat{z}\cdot\mathbf{f}_j(\mathbf{r}), g_{e,zd}(\mathbf{r},\mathbf{r}'), \nabla'\cdot\mathbf{f}_i(\mathbf{r}')\rangle \\
+ \; & i\omega\mu_m \langle \nabla\cdot\mathbf{f}_j(\mathbf{r}), g_{e,dz}(\mathbf{r},\mathbf{r}'), \hat{z}\cdot\mathbf{f}_i(\mathbf{r}')\rangle \\
+ \; & i\omega\mu_m \langle \nabla\cdot\mathbf{f}_j(\mathbf{r}), g_{e,dd}(\mathbf{r},\mathbf{r}'), \nabla'\cdot\mathbf{f}_i(\mathbf{r}')\rangle
\end{aligned} \tag{19}$$

where $\mathbf{f}_s = -\hat{z}\times\hat{z}\times\mathbf{f}$ is the horizontal projection of the basis function; the inner product is defined as $\langle \mathbf{f}(\mathbf{r})\cdot\mathbf{g}(\mathbf{r})\rangle = \int d\mathbf{r}\mathbf{f}(\mathbf{r})\cdot\mathbf{g}(\mathbf{r})$, and

$$g_{e,ss} = \frac{i}{4\pi}\int_0^\infty dk_\rho J_0(k_\rho\rho) F^{\mathrm{TE}} \frac{k_\rho}{k_{mz}} \tag{20}$$

$$g_{e,zz} = \frac{i}{4\pi}\int_0^\infty dk_\rho J_0(k_\rho\rho)\left(-\partial_z\partial_{z'}F^{\mathrm{TE}} + k_{mn}^2 F^{\mathrm{TM}}\right)\frac{1}{k_{mz}k_\rho} \tag{21}$$

$$g_{e,zd} = \frac{i}{4\pi}\int_0^\infty dk_\rho J_0(k_\rho\rho)\left(-\partial_z F^{\mathrm{TE}} - \frac{\mu_n}{\mu_m}\partial_{z'}F^{\mathrm{TM}}\right)\frac{1}{k_{mz}k_\rho} \tag{22}$$

$$g_{e,dz} = \frac{i}{4\pi}\int_0^\infty dk_\rho J_0(k_\rho\rho)\left(-\partial_{z'} F^{\mathrm{TE}} - \frac{\varepsilon_m}{\varepsilon_n}\partial_z F^{\mathrm{TM}}\right)\frac{1}{k_{mz}k_\rho} \tag{23}$$

$$g_{e,dd} = \frac{i}{4\pi}\int_0^\infty dk_\rho J_0(k_\rho\rho)\left(-F^{\mathrm{TE}} + \frac{\partial_z\partial_{z'}}{k_{nm}^2}F^{\mathrm{TM}}\right)\frac{1}{k_{mz}k_\rho}. \tag{24}$$

Similarly the matrix representation of $\mathscr{K}_{\mathrm{H}}$ operator is

$$\begin{aligned}
& \langle \mathbf{f}_j(\mathbf{r}), \mathscr{K}_H(\mathbf{r},\mathbf{r}'), \mathbf{f}_i(\mathbf{r}')\rangle \\
= \; & \tfrac{\mu_m}{\mu_n}\langle \nabla\cdot\mathbf{f}_j(\mathbf{r}), \mathbf{g}_{ce,ds}(\mathbf{r},\mathbf{r}'), \mathbf{f}_{is}(\mathbf{r}')\rangle \\
+ \; & \tfrac{\mu_m}{\mu_n}\langle \hat{z}\cdot\mathbf{f}_j(\mathbf{r}), \mathbf{g}_{ce,zs}(\mathbf{r},\mathbf{r}'), \mathbf{f}_{is}(\mathbf{r}')\rangle \\
+ \; & \tfrac{\mu_m}{\mu_n}\langle \mathbf{f}_{js}(\mathbf{r}), \mathbf{g}_{ce,sd}(\mathbf{r},\mathbf{r}'), \nabla'\cdot\mathbf{f}_i(\mathbf{r}')\rangle \\
+ \; & \tfrac{\mu_m}{\mu_n}\langle \mathbf{f}_{js}(\mathbf{r}), \mathbf{g}_{ce,sz}(\mathbf{r},\mathbf{r}'), \hat{z}\cdot\mathbf{f}_i(\mathbf{r}')\rangle
\end{aligned} \tag{25}$$

where

$$\mathbf{g}_{ce,ds}(\mathbf{r},\mathbf{r}') = \begin{bmatrix} -\sin\phi \\ \cos\phi \end{bmatrix} \frac{i}{4\pi}\int_0^\infty dk_\rho J_1(k_\rho\rho)\frac{\partial_z F^{\mathrm{TE}}}{k_{mz}} \tag{26}$$

$$\mathbf{g}_{ce,zs}(\mathbf{r},\mathbf{r}') = k_n^2 \begin{bmatrix} \sin\phi \\ -\cos\phi \end{bmatrix} \frac{i}{4\pi}\int_0^\infty dk_\rho J_1(k_\rho\rho)\frac{F^{\mathrm{TE}}}{k_{mz}} \tag{27}$$

$$\mathbf{g}_{ce,sd}(\mathbf{r},\mathbf{r}') = \frac{\mu_n}{\mu_m}\begin{bmatrix} \sin\phi \\ -\cos\phi \end{bmatrix} \frac{i}{4\pi}\int_0^\infty dk_\rho J_1(k_\rho\rho)\frac{\partial_{z'} F^{\mathrm{TM}}}{k_{mz}} \tag{28}$$

$$\mathbf{g}_{ce,sz}(\mathbf{r},\mathbf{r}') = k_{mn}^2 \begin{bmatrix} -\sin\phi \\ \cos\phi \end{bmatrix} \frac{i}{4\pi}\int_0^\infty dk_\rho J_1(k_\rho\rho)\frac{F^{\mathrm{TM}}}{k_{mz}} \tag{29}$$

#172033 - $15.00 USD Received 5 Jul 2012; revised 10 Aug 2012; accepted 11 Aug 2012; published 20 Aug 2012
(C) 2012 OSA

In Eqs. (26)–(29), $\phi = \arctan[(y-y')/(x-x')]$, and $J_1(k_\rho \rho)$ is the first order Bessel function.

As described above, the computation of the SER of the quantum emitter in a plasmonic system can be converted into a classical EM scattering problem. More specifically, the Green's function can be determined in the following way. We put an α-polarized Hertzian dipole to excite the structure, and calculate the scattered field at the same location by using the SIE with LMGF. Finally the Green's function (of the whole hybrid structure) can be deduced as

$$\mathrm{Im}\left[\bar{\mathbf{G}}_{\alpha\alpha}(\mathbf{r}_0,\mathbf{r}_0)\right] = \mathrm{Im}\left[\frac{\mathbf{E}^{\alpha}_{\mathrm{sca}}(\mathbf{r}_0)}{i\omega\mu(\mathbf{r}_0)}\right] + \mathrm{Im}\left[\frac{\mathbf{E}^{\alpha}_{\mathrm{inc,sec}}(\mathbf{r}_0)}{i\omega\mu(\mathbf{r}_0)}\right] + \frac{k_m}{6\pi} \tag{30}$$

The first term of the right-hand side is from the scattered field, the second term is from the secondary term of the incident field (due to the reflection and transmission of the layered medium), and the third term is from the primary term of the incident field (the field is singular but the imaginary part of Green's function is regular and has analytic solution).

Compared with the normal SIE based on FSGF, there are several advantages in our SIE scheme with LMGF in modeling the aforementioned complex multilayered plasmoinic system. First, the normal SIE needs to discretize nanoscatterers as well as the multilayered structure; thus the number of unknowns is huge, especially when considering that the structure is typically much larger than the nanoscatterers. Second, for accurately reproducing plasmonic effects, very fine mesh is required in modeling the nanoscatterers to capture the highly concentrated and localized field, hence multiscale discretization is required in the normal SIE and the condition of the matrix is bad. Finally, if the number of layers increases in certain optimizations, the equation has to be reformulated and the mesh needs to be regenerated; and hence the number of unknowns increases accordingly. However, for the scheme developed here, such problems can be overcome—only the surface of the nanoscatterers needs to be discretized, and increasing the number of layers does not introduce extra modeling complexity.

2.3. Evaluation of Sommerfeld integrals via discrete complex image method

The Sommerfeld integrals in Eqs. (20)–(24) involved normally have no analytic solution in the spatial domain and the numerical integration strategy is very inefficient. In this section we will apply the DCIM to accelerate the evaluation of Sommerfeld integrals in the LMGF. The Sommerfeld integrals in Eqs. (20)–(24) can always be expressed as an infinite integral of the following type

$$g(\rho) = \frac{i}{4\pi}\int_0^\infty dk_\rho \frac{k_\rho}{k_{mz}} J_0(k_\rho \rho)\tilde{g}(k_\rho). \tag{31}$$

If the integration kernel can be approximated by a series of complex exponentials,

$$\tilde{g}(k_\rho) = \sum_{i=1}^{M} a_i e^{ik_{mz}b_i} \tag{32}$$

by applying the Sommerfeld identity [27],

$$\frac{e^{ik_m r}}{r} = i\int_0^\infty dk_\rho \frac{k_\rho}{k_{mz}} J_0(k_\rho \rho) e^{ik_{mz}|z|},\ r = \sqrt{\rho^2+z^2} \tag{33}$$

the infinite integral can be evaluated in a closed form,

$$g(\rho) = \sum_{i=1}^{M} a_i \frac{e^{ik_m r_i}}{4\pi r_i},\ r_i = \sqrt{\rho^2+b_i^2}. \tag{34}$$

The complex exponential series can be obtained from the matrix pencil method [34] and will not be repeated here. As can be seen in Eq. (34), the LMGF consisting of infinite integrals finally

#172033 - $15.00 USD Received 5 Jul 2012; revised 10 Aug 2012; accepted 11 Aug 2012; published 20 Aug 2012
(C) 2012 OSA

becomes a series of FSGF with complex distances and amplitudes. Therefore, the computation can be made to be the same order as the free space problems.

For the Sommerfeld integrals in Eqs. (26)–(29), the DCIM can also be applied by using the following integration identity, which can be easily derived from the Sommerfeld identity in Eq. (33) and recurrence formula of Bessel function

$$\frac{1}{\rho}\left[e^{ik_m|z|}-|z|\frac{e^{ik_m r}}{r}\right]=\int_0^\infty dk_\rho J_1(k_\rho\rho)e^{ik_{mz}|z|} \tag{35}$$

One should note that the accuracy of the approximation in Eq. (32) is reasonably good for the near field calculation. However, it may loose accuracy in the far field regime due to the existence of surface wave poles (guided modes) or branch point singularity (lateral waves). This issue can be further addressed by proper deformation of the sampling path and the extraction of poles [35, 36].

3. Simulation results and discussion

To validate the accuracy of the SIE approach, we first test the scattering of a gold nanosphere in air, where analytic solution is available. The complex refractive index of gold is obtained by the Brendel-Bormann model [37]. The particle is illuminated by a normal incident plane wave at $\lambda = 510$ nm, the configuration is shown in Fig 2(a), and the near field along the observation line is shown in Fig. 2(b) and Fig. 2(c), compared with the one from MIE series [38]. The minor discrepancy occurs only at the boundary of the sphere, where the field is singular.

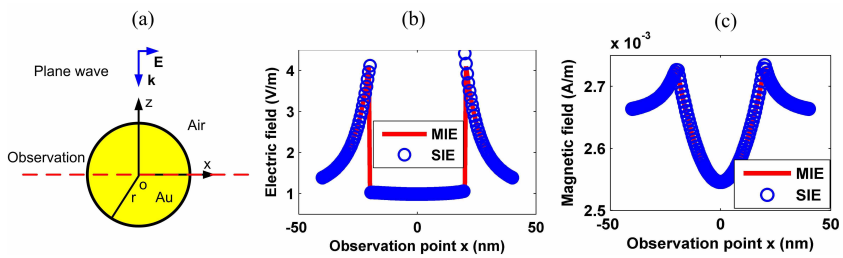

Fig. 2. (a) Configuration profile: a gold sphere is located in the air, illuminated by a normal incident plane wave, $r = 20$ nm, the observation line is shown by a dash line. (b) Near electric field, validated by MIE series. (c) Near magnetic field, validated by MIE series.

Next, we model the scattering of the gold nanosphere located in an air-gold-air substrate, excited by a z-polarized dipole, as shown in Fig. 3(a). In this case, no analytic solution is available. The accuracy is validated by an approximated model, where the substrate is truncated with a dimension of 600×600 nm, and the SIE based on FSGF is applied. The real part of the z-component of electric field $\mathrm{Re}\{E_z\}$ is calculated, which is proportional to the imaginary part of the Green's function $\mathrm{Im}\{G_{zz}\}$. The agreement of the two results is reasonably good, as shown in Fig. 3(b). After the validation we then calculate the SER of the configuration as shown in Fig. 3(a). The normalized SER with different polarizations of emitters are shown in Fig. 4(a) (x-polarized), and Fig. 4(b) (z-polarized), respectively. To clearly demonstrate the effect of the substrate, the results of the nanosphere in air and the substrate (the LMGF itself) are also calculated. It is observed that the vertically polarized dipole excites stronger field than the one from horizontally polarized dipole. This is because strong near-field evanescent wave coupling between sphere and substrate can be expected for z-polarized dipole imposed between the two metallic nanostructures. The localized plasmon from the nanosphere will strongly interact with the surface plasmon from the plate substrate resulting in a strong confinement and

#172033 - $15.00 USD Received 5 Jul 2012; revised 10 Aug 2012; accepted 11 Aug 2012; published 20 Aug 2012
(C) 2012 OSA

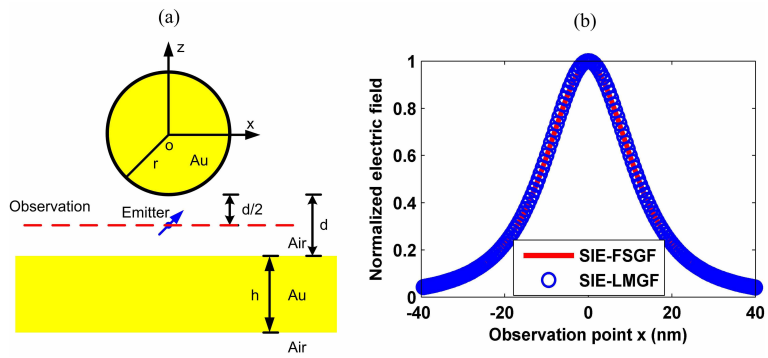

Fig. 3. (a) Configuration profile: a gold sphere is located in an air-metal-air substrate, excited by a z-polarized dipole, where $r = 20$ nm, $d = 20$ nm, $h = 30$ nm; (b) the real part of z-component of the electric field is calculated by our scheme (corresponding to the $\mathrm{Im}\{G_{zz}\}$), validated by an approximated model, where the substrate is truncated into a finite domain for discretization, and the SIE with FSGF is adopted.

large spontaneous decay rate. Particularly, constructive or coherent interferences by evanescent wave coupling in the case of z-polarized dipole makes the normalized SER of the hybrid system stronger than the summation of the nano sphere and the substrate. In Fig. 4(c), the normalized SER versus the distance between the nano particle and the metallic substrate is shown, where the SER decreases monotonically when the distance increases. This suggests that the near-field surface waves from plasmonic resonances contribute to the boosted SE in comparison with leaky waves in the middle or far field regions, which have weaker effects on SE. The near field distribution is also calculated at $\lambda = 510$ nm with z-polarized dipole as shown in Fig. 5. In Fig. 5(a), the mesh of the nanosphere is shown; in Fig. 5(b) and Fig. 5(c), the near scattered field of the nanosphere (in logarithmic scale) with and without the substrate is shown for comparison. The singular primary field of the dipole is subtracted for better demonstration. A strong E-field is concentrated at the gap between the nanosphere and substrate.

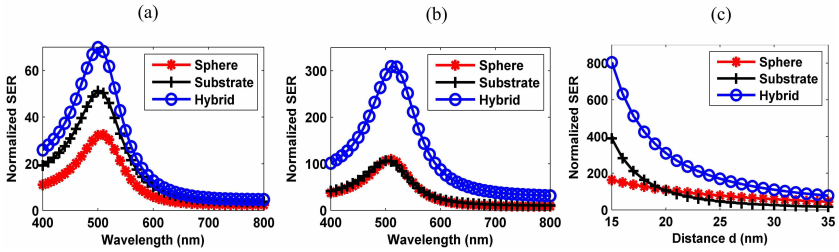

Fig. 4. (a) Normalized SER of a x-polarized emitter versus wavelength; (b) Normalized SER of a z-polarized emitter versus wavelength; (c) Normalized SER of a z-polarized emitter at $\lambda = 510$ nm versus distance.

Finally, to show the capability of our scheme in a general multilayered structure, the system for molecular detection or sensing in Fig. 6 is investigated. A triangular gold nanoantenna is embedded in an air-PMMA (poly methyl methacrylate)-ITO (indium tin oxide)-SiO_2 substrate. SE or Raman scattering from the molecular material can be amplified by the metallic structure. The dimension of the prism and the substrate is shown in Fig. 6(a), where the refractive indices are: $n = 1.49$ (PMMA), $n = 2$ (ITO), and $n = 1.47$ (SiO_2) [39]. The polarization of the dipole

#172033 - $15.00 USD Received 5 Jul 2012; revised 10 Aug 2012; accepted 11 Aug 2012; published 20 Aug 2012
(C) 2012 OSA

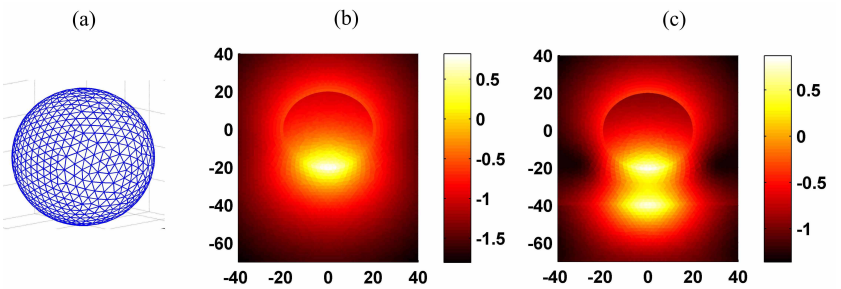

Fig. 5. (a) Mesh of the nano sphere; (b) Scattered near field distribution of the sphere with the absence of substrate (in logarithmic scale); (c) Scattered near field distribution of the sphere with the presence of substrate (in logarithmic scale).

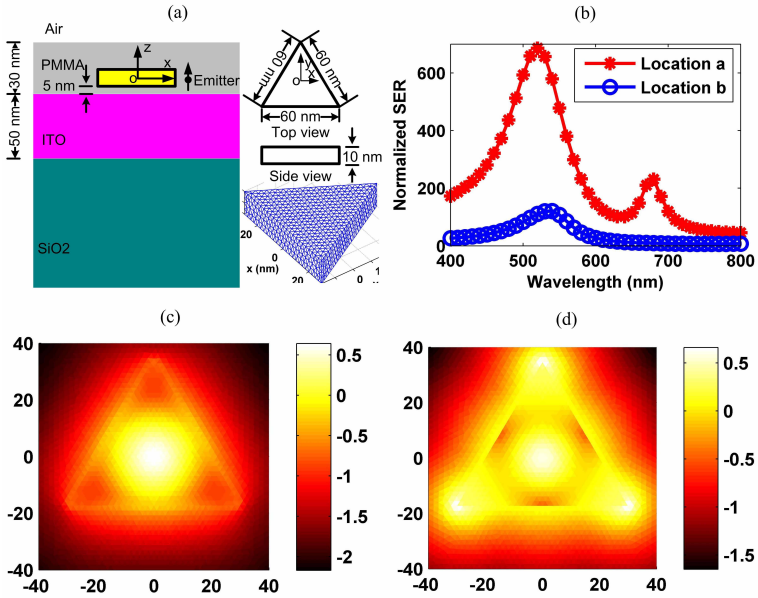

Fig. 6. (a) Configuration profile of the multilayered structure and mesh of the nano scatterer; (b) Normalized SER for different locations of z-polarized emitters: a: above the center of the prism $(0, 0, 10)$, b: around one corner of the prism $(-35, -17.32, 0)$; (c) Scattered near field distribution at the resonance peak of 520 nm; (d) Scattered near field distribution at the second resonance peak of 680 nm.

#172033 - $15.00 USD Received 5 Jul 2012; revised 10 Aug 2012; accepted 11 Aug 2012; published 20 Aug 2012
(C) 2012 OSA

is assumed to be directed at z direction. The normalized SER (with respect to the one in a homogeneous and unbounded PMMA space) for two different locations of the emitter is shown in Fig. 6(b). Location a is above the center of the prism $(0,0,10)$, and location b is around one corner of the prism $(-35,-17.32,0)$. It is observed that the SER is strongly location dependent, which should be taken into account in the design of the nanoantenna. For location a, there are two resonant peaks while for location b there is only one. The scattered near field distribution at the two resonance frequencies for the case of the location a is shown in Fig. 6(c) and Fig. 6(d), respectively. The primary field of the dipole is also subtracted and again logarithmic scale is adopted. As shown in Fig. 6(c), the near-field of the metallic prism is concentrated at the center region of its cross section at the resonance peak of 520 nm. The supported photonic-like mode contributes the boosted SE. Furthermore, the whole prism is fully excited at the second resonance peak of 680 nm as depicted in Fig. 6(d). The sharp E-field hotspots are focused on the tips of the prism induced by the plasmonic and lightning-rod effects. The dipole, with different positions and orientations, enables distinguished eigenstates of the nanoantenna system excited involving plasmonic and photonic-like modes. As a result, the enhanced SER shows position and polarization dependent features. All the numerical simulations except for the approximated validation model mentioned above are run on a personal computer with 2.66 GHz processor and 2 Gb memory, without the necessity to invoke super computers.

4. Conclusion

A surface integral equation method with layered medium Green's function has been proposed to study the spontaneous emission of a quantum emitter in a complex multilayered plasmonic system. Different metallic nanoscatterers are incorporated to the multilayered system to boost the spontaneous emission, which is commonly encountered in various optical applications. The spontaneous emission rate is obtained from the Green's function of the whole system and solved by using a classical full-wave electromagnetic solver. The discrete complex image method is further applied to expedite the computation. This work offers an accurate and efficient simulation tool for producing and understanding the spontaneous emission in complex multilayered plasmonic systems.

Acknowledgments

This work was supported in part by the Research Grants Council of Hong Kong (GRF 711609, 711511 and 713011), in part by the University Grants Council of Hong Kong (AoE/P-04/08).